



1 **Low-temperature thermochronology and its**
2 **geological significance in the central and northern**
3 **section of the western margin of the Ordos Basin**

4 Guangyuan Xing^{1,2}, Zhanli Ren^{1,2*}, Kai Qi^{1,2}, Sasa Guo^{1,2}, Yanzhao Liu^{1,2},
5 Ying Zhang³, Huaping Lan⁴

6 ¹ *Department of Geology, Northwest University, Xi'an 710069, China;*

7 ² *State Key Laboratory of Continental Dynamics, Northwest University, Xi'an 710069,*
8 *China;*

9 ³ *Research Institute of Yanchang Petroleum(Group) Co.Ltd., Xi'an 710075, China;*

10 ⁴ *Research Institute No. 203 of Nuclear Industry, Xi'an 710000, China*

11 Correspondence to: Zhanli Ren

12 E-mail: renzhanl@nwu.edu.cn

13 **Abstract:** The study of low-temperature thermochronology at plate edges
14 provides favorable constraints for regional tectonic evolution and surface
15 processes. Based on the existing thermochronological data of multiple
16 cooling events since the Mesozoic era, we conducted apatite fission track
17 and apatite (U-Th)/He studies on drilling samples from the middle and
18 northern parts of the western margin of the Ordos Basin, revealing the
19 uplift and cooling history and differences in the middle and northern parts
20 of the western margin of the Ordos Basin. The new thermal history
21 simulation results show that the Zhuozishan Mountain(Mt.) part
22 experienced large-scale uplift in the Late Jurassic (160Ma-150Ma), slow
23 uplift at 130Ma-30Ma and severe uplift after 30Ma; The Taole -
24 Hengshanbao part began to uplift at 155Ma-145Ma, slowly uplifted at
25 145Ma-30Ma, and then violently uplifted; The Majiatan - Huianbao part
26 experienced large-scale uplift at 158Ma-137Ma, with a slightly slower



27 uplift rate at 137Ma-110Ma, and entered a severe uplift stage again at
28 70Ma-50Ma. The Late Jurassic tectonic uplift indicated by
29 thermochronology corresponds to the formation of the western margin
30 thrust fold structure, with the northern and southern sections starting
31 earlier and the middle section starting slightly later. This is related to the
32 different tectonic evolution and stress in their location, and the
33 differences in uplift rate and time may be related to the impact of multiple
34 Yanshanian orogeny on the region.

35 **Keyword:** Ordos Basin; North China Block; Plate convergence;
36 Low-temperature thermochronology; Yanshanian orogeny

37

38 **1 Introduction**

39 The North China Craton, as one of the oldest cratons in the world,
40 has a long history spanning 3.8 billion years (Zhai, 2010; Zhang et al.,
41 2018). Having undergone prolonged and complex tectonic evolution, it
42 records nearly all major tectonic events from ancient to the present,
43 especially preserving multi-phase evolutionary remnants since 1.8 billion
44 years ago (Peng et al., 2022). The Ordos Block is part of the North China
45 Craton and one of its core geological units (Bao et al., 2019; Zhai, 2021).
46 The present-day Ordos Basin, in a narrow sense, is located in the western
47 part of the North China Craton. It was formed on the foundation of the
48 North China Craton through multiple phases of transformation,



49 particularly since the Mesozoic, eventually developing into a residual
50 intracratonic basin (Ren et al., 1995; Zhai, 2021). This basin is
51 superimposed on a large Paleozoic basin, making it a composite basin
52 (Liu et al., 2005). The Ordos Basin contains the most complete
53 sedimentary strata in the North China region and is rich in multiple
54 energy resources, including oil, gas, coal, and uranium, making it a highly
55 resource-abundant basin.


56 The thrust belt along the western margin of the Ordos Basin spans
57 across different tectonic units, including the North China Craton, the Alxa
58 Block, the Central Asian Orogenic Belt, the Qinling Orogenic Belt, and
59 the northeastern edge of the Tibetan Plateau (Fig.1). It is one of the
60 regions with the most intense tectonic deformation within the Chinese
61 mainland since the Mesozoic, recording numerous intracontinental
62 deformation and orogenic events since the Phanerozoic. Additionally, the
63 western margin of the Ordos Basin lies in the northern segment of the
64 North-South Tectonic Belt of China, connecting different tectonic units
65 between the western and eastern parts of northern China (Dong et al.,
66 2021).

67 The study area is located in the central-northern section of the
68 western margin of the Ordos Basin (Fig. 1). Influenced by multiple
69 tectonic movements, the region has a complex evolutionary history, with
70 several large-scale, north-south-oriented thrust faults. In general, the



71 northern part of this tectonic belt is believed to result from interactions
72 between adjacent tectonic blocks. Over the years, various scholars have
73 conducted extensive research on the structural characteristics and
74 properties of the northern section of the western margin (Yang et al., 1986;
75 Tang et al., 1988, 1992; Gan et al., 1990; Liu et al., 1995; Zhao et al.,
76 1990), its formation mechanisms (Liu et al., 1997; Liu et al., 2005;
77 Ouyang et al., 2012; Yang et al., 2011; Yang et al., 2006, 2008; Zhao et al.,
78 2003, 2006, 2007a, c), and provenance (Jiang et al., 2019). Regarding the
79 overall uplift process along the western margin, many scholars, using
80 apatite fission track methods, suggest that the uplift in the southern
81 section of the western margin began in the Middle to Late Jurassic (Chen
82 et al., 1999, 2007; Gao et al., 2000; Zhang et al., 2000; Zhao et al., 2003,
83 2006, 2007b; Zhao et al., 2017; Li et al., 2019; Ma et al., 2019; Peng
84 Heng, 2020; Tian et al., 2023). Due to the presence of an east-west
85 transfer zone in the Qingtongxia-Majiatan area, the western margin can
86 be divided into three distinct tectonic systems: southern, central, and
87 northern, based on differences in structural characteristics and
88 sedimentation (Zhao et al., 2006). In the northern part of the western
89 margin, including the Helanshan Mt. region, low-temperature
90 thermochronology studies are relatively scarce and have mainly focused
91 on the Helanshan Mt. area (Ma et al., 2019; Zhao et al., 2007a; Liu, 2010),
92 the Zhuozishan Mt. region (Zhuo, 2015; Li, 2006), the 38°N Tectonic



93 Belt and adjacent areas (Gao, 2014; Zhao et al., 2007b, c; Ma et al., 2019;
94 Li, 2019), and drilling wells such as LS1 well, T1 well, and TS1 well (Ren
95 et al., 1995). 

96 From the limited published thermochronological data, it is evident
97 that the study area entered an uplift evolution stage during the Mesozoic,
98 but the timing and rate of uplift vary across different regions. The
99 structural differences between the basin margin and the interior have not
100 been well clarified. Current research lacks a comprehensive perspective
101 and does not provide a systematic understanding of tectonic events in the
102 central-northern section of the western margin of the Ordos Basin since
103 the Mesozoic. This greatly limits further insights into the overall tectonic
104 evolution of the area and poses significant challenges for deeper research
105 into intracontinental deformation in the basin and its surrounding regions.

106 This study utilizes low-temperature thermochronology methods,
107 combined with thermal history modeling and existing geological evidence,
108 to precisely constrain the uplift and cooling history of the central-northern
109 section of the western margin of the Ordos Basin. The research helps
110 improve our understanding of the evolution and tectonic processes in this
111 region since the Mesozoic, ~~providing important evidence for studying the~~
112 ~~formation and evolution of the Ordos Basin and the tectonic deformation~~
113 ~~that occurred along the basin's margins during the Mesozoic.~~ Additionally,
114 it offers a foundational reference for future oil and gas exploration efforts

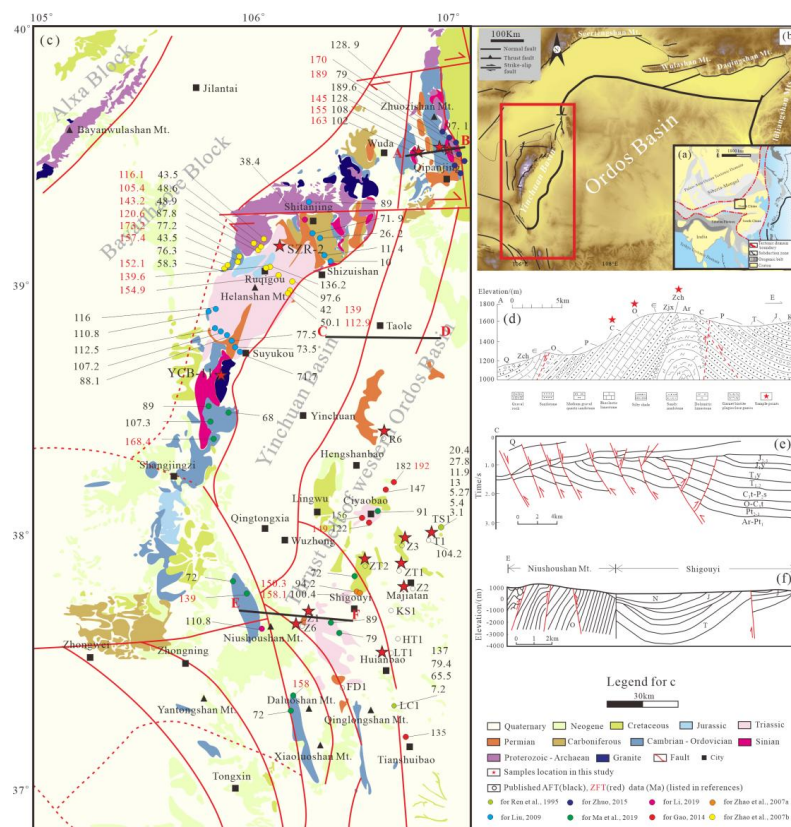


115 ~~in the western margin of the basin.~~

116 **2 Geological setting**

117 The Ordos Basin, as one of the key geological ~~units~~ of the North
118 China Craton, is a large composite basin formed during different periods,
119 ~~across varying extents, and under diverse geodynamic settings (Ren et al.,~~
120 ~~2020). Based on the basin types and tectonic evolutionary characteristics~~
121 ~~of different eras, the basin's evolution~~ can be divided into several stages:
122 Archean-Paleoproterozoic basement formation ~~stage~~, Mesoproterozoic -
123 Neoproterozoic rift basin development ~~stage~~, Early Paleozoic stable
124 continental margin sedimentation ~~stage~~, Late Paleozoic to Middle Triassic
125 intracratonic basin evolution ~~stage~~, Late Triassic to Jurassic
126 intracontinental depression basin evolution ~~stage~~, Early Cretaceous
127 westward contraction of the depression basin, Late Cretaceous to
128 Cenozoic significant uplift, Formation of Cenozoic fault-depression
129 basins in the surrounding areas (Liu et al., 2006; Ren et al., 2020; Li,
130 2006).

131 In order to more precisely define the differences in the later uplift
132 and cooling processes, this article further divides the research area into
133 the Zhuozishan Mt. part, the Taole-Hengshanbao part, and the
134 Majiatan-Huianbao part.



135
 136 Fig.1 (a) Tectonic setting of China (modified from Peng et al., 2019), (b) Digital
 137 elevation model of the Ordos basin (modified from Shi et al., 2020), (c) Geological
 138 map of the central-northern section of the western margin of the Ordos Basin
 139 (modified from Ma, 2019) and compilation of previously published low-temperature
 140 thermochronology data, (d) W - E trending simplified geological profile A-B studied
 141 in this article (modified from Zhuo, 2015), (e) W - E trending simplified geological
 142 profile C-D studied in this article (modified from Zhao, 2006), (f) W - E trending
 143 simplified geological profile C-D studied in this article (modified from Ma, 2019).

144 In the Zhuozishan Mt. part, faults thrust from west to east, consisting
 145 of the Bayin'aobao thrust sheet, the Wuhushan thrust sheet, the Gandel
 146 Mountain thrust sheet, and the Zhuozishan Mt. thrust sheet. The
 147 Zhuozishan anticline is located near the basin, with an east-west length of
 148 approximately 10 km. The core of the anticline exposes older strata, with
 149 Archean granitic gneiss of the Qianlishan Group at its core. Moving



150 westward, it sequentially exposes the Changcheng System Huangqikou
151 Formation, Jixian System Wangquankou Formation, Cambrian Taosigou
152 Formation, Hulusitai Formation, Zhangxia Formation, Abuqiehai
153 Formation, Ordovician Sandaokan Formation, Zhuozishan Formation,
154 and the Permian Shanxi Formation and Shihezi Formation (Fig. 1d).

155 In this study, the central part of the research area is defined as the
156 Taole-Hengshanbao part. Overall, the structural line in this region is
157 distributed in a nearly north-south orientation, and its structural
158 characteristics differ from those of the Zhuozishan Mt. part. The faults in
159 this area exhibit high-angle thrusting from east to west, characterized by a
160 series of imbricated thrust faults (Fig. 1e). Additionally, this part
161 corresponds to the Yinchuan Graben to the west, and their tectonic
162 evolution is closely related (Zhao, 2006).

163 The Majiatan-Huianbao part is characterized by typical thrust nappe
164 structures, with four west-dipping thrust faults developing from west to
165 east. These faults exhibit steep upper angles and gentle lower angles.
166 From west to east, the major thrust sheets include the Weizhou thrust
167 sheet, Qinglongshan thrust sheet, Shigouyi thrust sheet, and Yandunshan
168 thrust sheet. Among them, the Shigouyi thrust sheet, in an anticlinal form,
169 is situated between the Qingshanlong Fault and the Huianpu-Shajingzi
170 Fault (Fig. 1f).

171 In the Hengshanbao area, east-dipping faults are dominant, while the



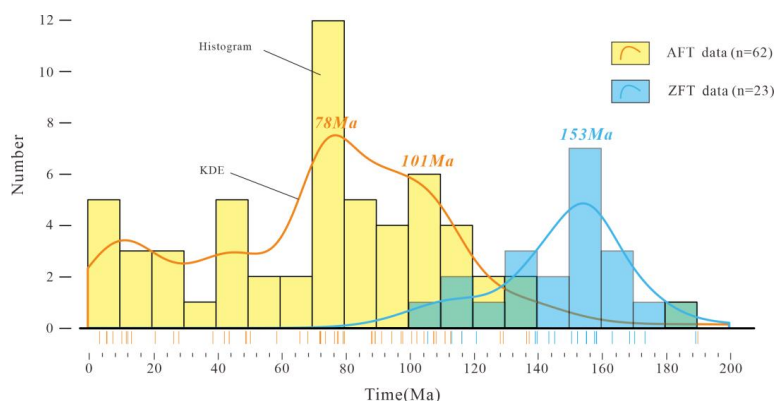
172 Majiatan-Huianbao part primarily features large west-dipping faults. The
173 38°N structural zone between these regions plays a regulatory role, and
174 the different structural styles on both sides have created distinct types of
175 traps. This has resulted in the concentration of oil and gas fields along the
176 western margin of the basin, particularly in the Shigouyi and Majiatan
177 areas (Gao, 2014; He et al., 2021).

178 **3 Sampling strategy and methodology**

179 **3.1 Previous thermochronological data**

180 This study collected a total of 85 published low-temperature
181 thermochronology data from the western margin of the Ordos Basin,
182 specifically between the Zhuozishan Mt. and the Tianshuibao, including
183 62 apatite fission track ages and 23 zircon fission track ages (Fig. 2).
184 Samples with higher mineral closure temperatures exhibit older apparent
185 ages. The ages of apatite samples range from 3.1 Ma to 189.6 Ma, while
186 zircon fission track ages range from 105.4 Ma to 192 Ma. These findings
187 indicate a long cooling history and a complex uplift process in the study
188 area. Based on the collected data, we plotted histograms and kernel
189 density estimation curves, revealing that the density peaks for apatite
190 fission tracks and zircon fission tracks are at 78 Ma, 101 Ma, and 153 Ma,
191 respectively.

192



193

194 Fig.2 Histogram and kernel density estimation (KDE) plot of published
195 geochronological dates in the central-northern section of the western margin of the
196 Ordos Basin. The bandwidth and bin width are both set to 10 Ma for all plots when
197 the graph is drawn.

198

In summary, previous thermochronological data indicate that
199 multiple cooling events have occurred in the region since the Mesozoic
200 era (Ren et al., 1995; Zhao et al., 2007a, b; Liu, 2010; Zhuo, 2015; Gao,
201 2014; Li, 2019; Ma et al., 2019). However, due to a lack of chronological
202 methods, the cooling history of the study area during the late Cenozoic
203 has not been well constrained.

204

3.2 Sample collection and experimental methods

205

This study applies thermochronology to constrain the spatiotemporal
206 evolution of the upper few kilometers of the lithosphere. As one of the
207 most widely used and effective thermochronological methods (Gleadow
208 and Seiler, 2015; Peng, 2020), apatite fission track analysis is sensitive to
209 temperature variations in the range of 60°C to 120°C (the partial
210 annealing zone), while apatite (U-Th)/He dating is suitable for defining
211 the time-temperature history in the range of 40°C to 75°C (Ketcham,



212 2005; Gallagher, 2012; Flowers et al., 2015; Farley et al., 2002).

213 To systematically study the differences in uplift and cooling ~~in the~~
214 ~~central-northern part of the western margin~~, the relationship between
215 structural evolution at the basin edge and within the basin, and to address
216 the current gaps in thermochronology in the research area, this study
217 collected 16 valuable samples, including 11 core samples from 9 drilling
218 wells and 5 field outcrop samples. ~~Apatite fission track analysis and~~
219 ~~apatite (U-Th)/He dating were employed for chronological analysis.~~ The
220 samples are well-distributed across the entire **central-northern region of**
221 **the western margin** and are representative **of various stratigraphic levels.**
222 **After obtaining the samples, apatite was separated using conventional**
223 **heavy liquid and magnetic separation methods.**

224 ~~All 16 samples were analyzed using apatite fission track (AFT)~~
225 ~~methodology.~~ After selecting mineral grains, the samples were prepared,
226 tested, and analyzed at the Petroleum Thermochronology Laboratory in
227 the Department of Geology at Northwest University. The calculation
228 method for AFT ages follows Hasebe et al. (2004), and ages were
229 analyzed using RadialPlotter software (Vermeesch, 2009) (Fig.3, **4a**).
230 Additionally, the HeFTy software was utilized to simulate the cooling
231 history (Ketcham, 2005).



232 Fig.3 AFT age Radial plots for samples (WHM-5, 8, and 12 are the data that the
 233 author will soon publish, while the rest are newly published data in this paper).
 234

235 Additionally, following three criteria—selecting well-formed, pure
 236 grains and ensuring that the crystal dimensions perpendicular to the c-axis
 237 exceed 60-70 μm—apatite grains from samples Z1-33 and ZT2-18 were
 238 chosen under a high magnification (160x) binocular microscope for
 239 (U-Th)/He (AHe) dating. This experiment was conducted at the
 240 Argon-Argon and U-Th-He Geochronology Laboratory of the Institute of
 241 Geology and Geophysics, Chinese Academy of Sciences. ~~The thermal~~
 242 ~~history of the samples was also modeled using HeFTy software (Ketcham,~~
 243 ~~2005).~~



244 4 Results

245 4.1 Low-temperature thermochronology results

246 4.1.1 Zhuozishan Mt. part

247 The AFT central ages of the three sandstone samples from the
248 Zhuozishan Mt. part (WHM-5, WHM-8, WHM-12) are 153 ± 6.6 Ma,
249 125 ± 6 Ma, and 135 ± 5 Ma, respectively, all of which are significantly
250 younger than the stratigraphic ages ~~from which the samples were derived.~~

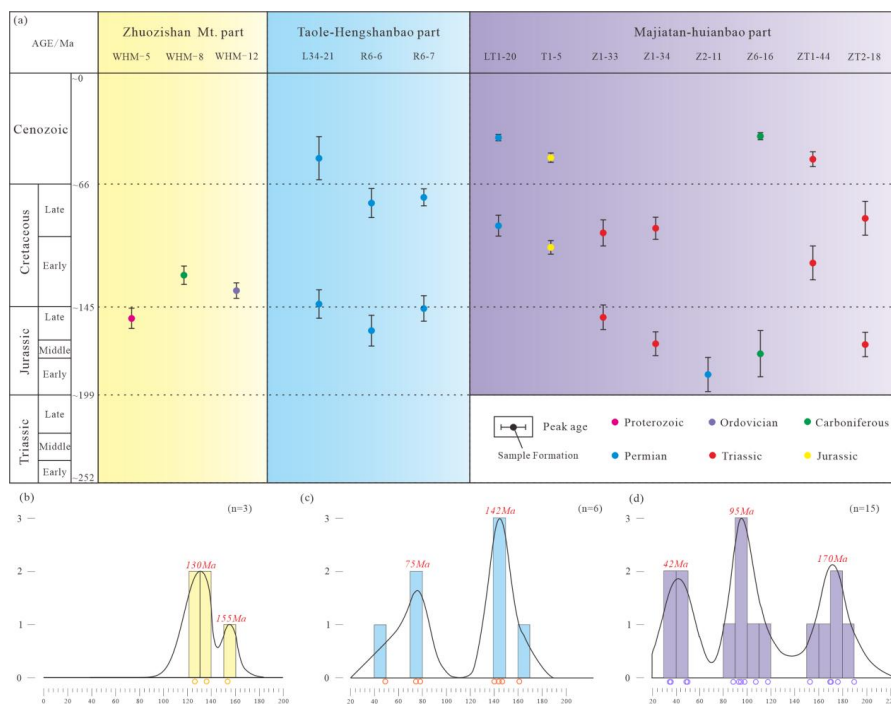
251 The average track lengths are 12.16 ± 1.54 μm , 11.43 ± 1.55 μm , and
252 13.3 ± 1.7 μm , all of which are shorter than the spontaneous track original
253 length of 16.3 ± 0.9 μm , indicating that the samples have undergone
254 annealing and cooling processes. All three samples passed the χ^2 test
255 ($P(\chi^2) > 5\%$), suggesting that each sample contains a single age
256 component. The RadialPlotter software provided single ages of 153 ± 6.6
257 Ma, 126.1 ± 8.6 Ma, and 134.7 ± 7.9 Ma (Fig. 4b), which are consistent
258 with the central ages within a certain error range. The age of 153 ± 6.6 Ma
259 may represents a tectonic event in the Late Jurassic, ~~while~~ 134.7 ± 7.9 Ma
260 may corresponds to an early tectonic event in the Early Cretaceous, and
261 126.1 ± 8.6 Ma may indicates a tectonic event in the Late Early
262 Cretaceous.

263 4.1.2 Taole-Hengshanbao part

264 The AFT central ages of the two samples from well R6 (R6-6 and
265 R6-7) are 140.4 ± 15.7 Ma and 115.3 ± 10.2 Ma, with average track lengths



266 of $11.66 \pm 1.02 \mu\text{m}$ and $12.1 \pm 1.52 \mu\text{m}$, respectively. The AFT central age
267 of the sample from well L34 (L34-21) is $130 \pm 19.8 \text{ Ma}$. In the Helanshan
268 Mt. area, the AFT central ages of samples SZR-2 and YCB-11 are
269 $95.2 \pm 14.8 \text{ Ma}$ and $95.4 \pm 3.7 \text{ Ma}$, with average track lengths of 12.01 ± 1.68
270 μm and $12.88 \pm 1.11 \mu\text{m}$, respectively. The AFT central ages of these five
271 samples in this region are significantly younger than the stratigraphic
272 ages from which they were derived, indicating that the samples have
273 undergone annealing and cooling processes. Only the YCB-11 sample
274 passed the χ^2 test, with the RadialPlotter software providing a single peak
275 age of $95.2 \pm 3.2 \text{ Ma}$. The remaining four samples did not pass the χ^2 test,
276 suggesting that each sample contains at least two age populations. The
277 RadialPlotter software (Vermeesch, 2009) was used to decompose the
278 ages, and these peak ages record potential tectonic activities in this region
279 during the Late Jurassic, early Early Cretaceous, late Early Cretaceous,
280 Late Cretaceous, and Eocene epochs (Fig. 4c).



281

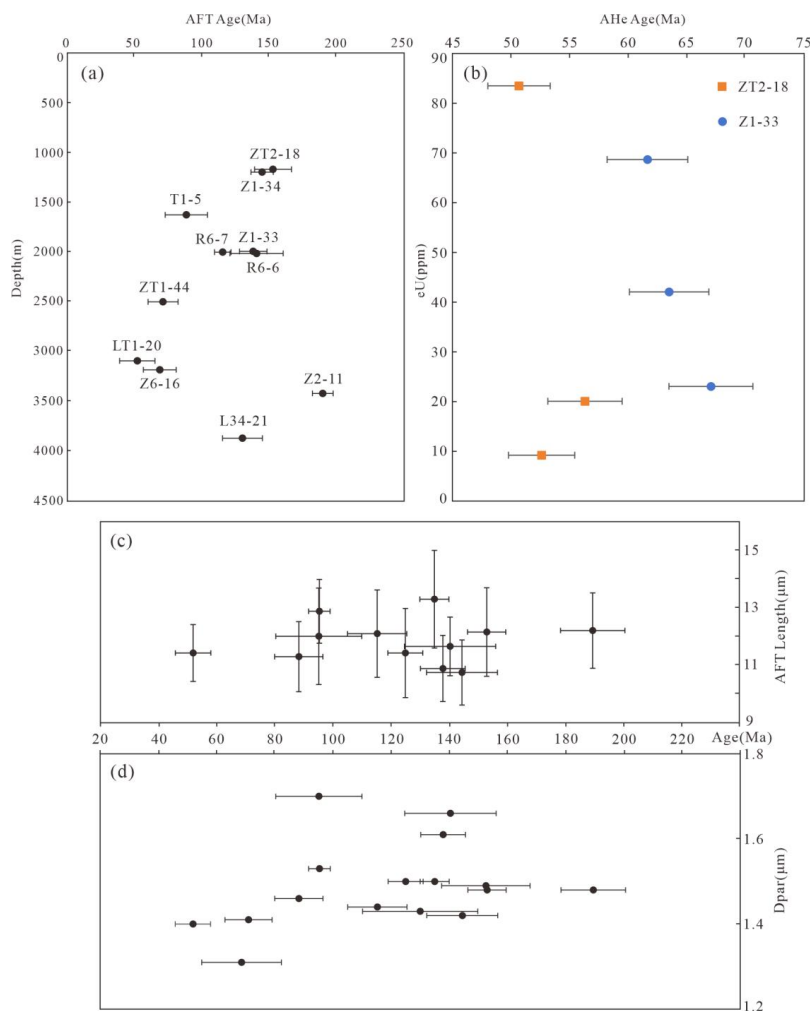
282 Fig.4 (a) The peak age distribution map of the three areas in the study region. (b),
 283 (c), (d), Histogram and kernel density estimation (KDE) plot of new **geochronological**
 284 dates in Zhuozishan Mt. part, Taole-Hengshanbao part, and Majiatan-Huianbao part.

285 4.1.3 Majiatan-Huianbao part

286 Due to this region being a sweet spot for oil and gas exploration, a
 287 large number of drilling samples are available. Except for sample Z2-11,
 288 which passed the χ^2 test, the remaining samples did not pass the test. The
 289 ages range from 35.6 to 189.5 Ma and were statistically divided into three
 290 peak values: 42 Ma, 95 Ma, and 170 Ma. All of these ages are
 291 significantly younger than the stratigraphic ages ~~from which they were~~
 292 ~~derived~~, indicating that they have undergone uplift and cooling processes
 293 (Fig. 4d). The three single-grain AHe ages for sample Z1-33 range from
 294 61.64 Ma to 67.06 Ma, while the three single-grain AHe ages for sample



295 ZT2-18 range from 50.69 Ma to 56.31 Ma, with no significant correlation
296 to eU, recording late uplift and cooling events (Fig. 5).



297
298 Fig.5 Relationships between AFT Age and (a) depth, (c) AFT length, and (d)
299 Dpar, (b) relationships between AHe age and eU.

300 In addition, the correlation between track length and AFT age
301 indicates a complex cooling history in the region. Considering the
302 different annealing dynamics (Ketcham et al., 2007), the chemical
303 composition of the grains may influence the AFT age and length (Carlson



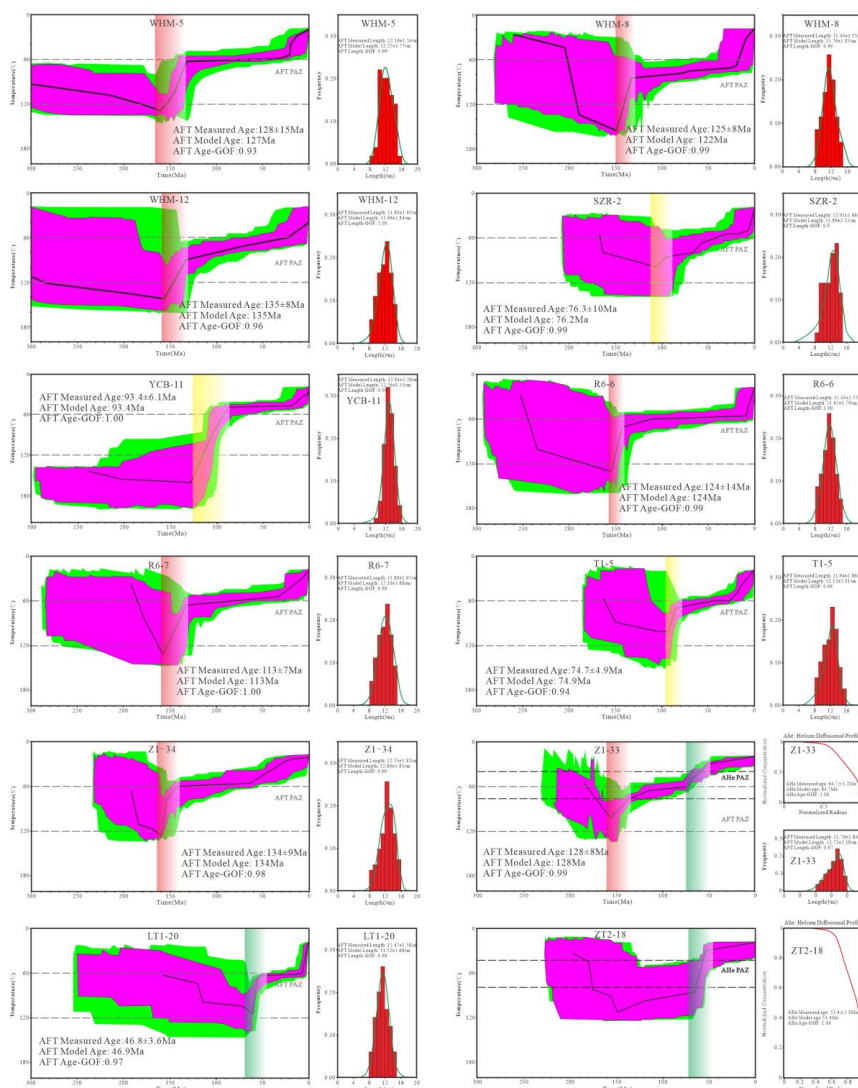
304 et al., 1999; Barbarand et al., 2003). However, the Dpar values in the
305 samples range from 1.31 μm to 1.70 μm , showing minimal variation and
306 no significant correlation with the AFT ages. This suggests that the
307 influence of chemical composition on AFT age is either minimal or
308 nonexistent.

309 **4.2. Thermal history modeling**

310 Due to the complexity of annealing processes, the measured
311 apparent ages lack any practical geological significance (Flowers et al.,
312 2015). By utilizing the measured ages, track lengths, Dpar values, and
313 other parameters, this thermal history can be inversely modeled (Ketcham,
314 2005). In this study, HeFTy version 1.6.7 was used for inverse modeling
315 (Ketcham, 2005), in conjunction with all available low-temperature
316 thermochronology data for path analysis. The Ketcham (2005)
317 multi-dynamic annealing model was selected for the inversion simulation,
318 along with the corrected confined track lengths. The original confined
319 track length was set at 16.3 μm , and the present-day surface temperature
320 was 20°C. The goodness-of-fit parameter (GOF) was used to indicate
321 how well the simulation results matched the actual measurements; a
322 higher value signifies a better fit. When the GOF value obtained from the
323 simulation exceeds 0.05, it indicates that the simulation results are
324 acceptable, while a GOF value greater than 0.5 indicates a very good
325 match. The simulated ages and lengths both had GOF values greater than



326 0.5 and close to 1, suggesting that the simulation results closely aligned
327 with the measured values.



328
329 Fig.6 Thermal history inverse modeling calculated by HeFTy (Ketcham, 2005),
330 using the model of Ketcham et al. (2007) and Flowers et al. (2009). HeFTy modeling
331 tests possible t - T curves by using the Monte-Carlo inverse modeling approach.
332 Shaded parts of different colors represent different cooling periods.

333 Among the 16 samples, 12 with more extensive length information
334 were selected for thermal history simulation, representing a broad



335 distribution across the study area to assess their potential thermal history
336 and determine their uplift cooling times. The goodness-of-fit parameters
337 for both length and age in this simulation were above 0.90, indicating a
338 good fit. The inverted time-temperature paths are shown in Fig. 6.


339 **5 Discussion**

340 From the thermal history simulation paths, the uplift initiation times
341 for the three sample sections generally fall in the late Jurassic; however,
342 there are still differences. The middle Taole-Hengshanbao part was
343 uplifted later, while the northern and southern parts were uplifted earlier,
344 which is related to the tectonic evolution and stress of their respective
345 locations. Additionally, the uplift intensity varies from east to west across
346 the regions. For example, in the northern part, the uplift rate of the
347 Changcheng System, which is closer to the core of the syncline on the
348 eastern side of the Zhuzishan syncline, is faster than that of the Paleozoic
349 strata on the western side. The samples from the southern part indicate
350 that uplift occurred earlier in the western samples compared to those in
351 the eastern side. These observations are closely linked to the reverse
352 thrusting and imbrication along the western margin (Fig. 7).

353 **5.1 Uplift Process Differences and Geological Responses in the** 354 **North-Central Western Margin Constrained by Low-Temperature** 355 **Thermochronology**

356 **5.1.1 Zhuozishan Mt. part**

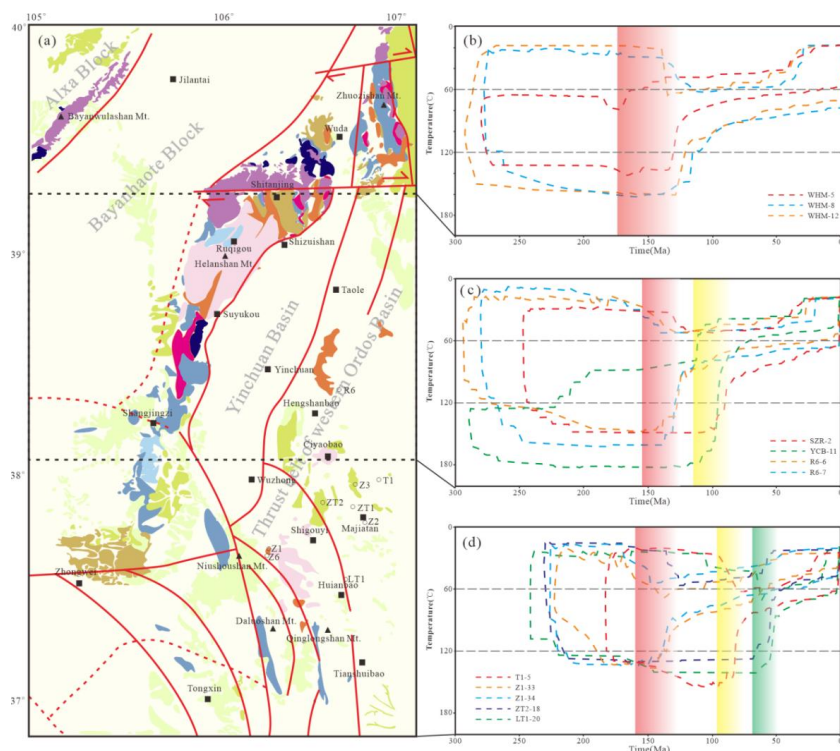


357 The thermal history inversion results for the three samples from the
358 northern Zhuozishan Mt. part indicate that the region underwent three
359 major uplift stages after the Mesozoic: Late Jurassic (160 Ma - 150 Ma),
360 This marks the first major uplift stage in the area, with an average uplift
361 rate of ca. 45 m/Ma and an average cooling rate of ca. 2°C/Ma. This uplift
362 corresponds to the early stages of the Yanshanian orogeny in the region,
363 triggering reverse thrusting and imbrication, as evidenced by the
364 inversion results of all three samples. Stratigraphically, the Late Jurassic
365 deposits are largely absent in the study area, with the Middle Jurassic
366 Anding Formation directly in contact with the Lower Cretaceous strata;
367 Early Cretaceous (130 Ma - 30 Ma), This stage represents a period of 
368 slow cooling, suggesting the absence of significant tectonic events during
369 this time. The timing and uplift differences among the samples during this
370 phase may reflect the varying effects of different episodes of the
371 Yanshanian orogeny (stages II, III, and IV) on the region; Cenozoic (since
372 ca. 30 Ma), The most recent uplift stage is associated with the Himalayan
373 orogeny, which caused further significant uplift in the region.

374 In terms of the spatial distribution of the Zhuzishan anticline (Fig.
375 1d), the WHM-5 sample from the Changcheng System on the eastern side
376 of the anticline entered and exited the partial annealing zone earlier than
377 the WHM-8 sample from the Taiyuan Formation on the western side. This
378 sequence aligns with the recorded ages. Additionally, the eastern side,



379 closer to the core of the anticline, exhibits a faster uplift rate in the
380 Changcheng System compared to the Paleozoic strata on the western side,
381 with the Ordovician strata showing intermediate uplift rates. Combined
382 with previous analyses of Mesozoic samples on the eastern flank of the
383 Zhuzhishan anticline, the general conclusion is that the core of the
384 anticline experienced rapid uplift, while the flanks uplifted more slowly,
385 indicating a differential uplift process (Zhuo, 2015).



386
387 Fig.7 Summary of all available thermochronology modeling history (envelope
388 path) for central-northern section of the western margin of the Ordos Basin.

389 5.1.2 Taole-Hengshanbao part

390 In the Taole-Hengshanbao part, two samples from well R6 have peak
391 ages of 161 Ma, 146 Ma, 78 Ma, and 74 Ma, suggesting possible tectonic



392 events during the Late Jurassic and Late Cretaceous. The thermal history
393 models of both samples show similar results, indicating three phases of
394 uplift: Late Jurassic (155 Ma-145 Ma), a period of significant uplift
395 begins; Early Cretaceous (145 Ma-30 Ma), this phase is characterized by
396 slow uplift; Cenozoic (ca. 30 Ma-), a period of intense and rapid uplift
397 occurs. The ages recorded in samples R6-6 and R6-7 are consistent within
398 the error range. The slight differences in their AFT model results arise
399 because R6-6 was located deeper, meaning it exited the partial annealing
400 zone later than R6-7 during uplift. This caused the AFT age constraints
401 for R6-6 to be slightly younger.

402 The uplift in this part is related to the uplift in the neighboring
403 Helanshan Mountain region and the intense faulting and subsidence in the
404 Yinchuan Graben. The thermal history models of the two Helanshan
405 Mountain samples (SZR-2 and YCB-11) show a spatial pattern: the
406 southern YCB-11 sample experienced rapid cooling at the end of the
407 Early Cretaceous (130 Ma-95 Ma), followed by slow cooling until the
408 Eocene (~35 Ma), after which it rapidly uplifted to the surface. The
409 northern SZR-2 sample, however, shows a delayed cooling history, with
410 cooling events occurring primarily after the Early Cretaceous. The uplift
411 pattern, with earlier uplift in the south and later uplift in the north, aligns
412 with previous studies on the Helanshan Mountain region (Ma et al.,
413 2019).



414 **5.1.2 Majiatan-Huianbao part**

415 In the southern, Majiatan-Huianbao part, two samples from well Z1
416 (Z1-33 and Z1-34) indicate that uplift in the well began during the Late
417 Jurassic (ca. 160 Ma). Combined AFT and AHe inversion results show
418 that sample Z1-33 experienced rapid uplift between 158 Ma and 137 Ma,
419 followed by slower uplift from 137 Ma to 110 Ma, and then entered
420 another phase of intense uplift between 70 Ma and 50 Ma. Sample Z1-34,
421 constrained only by AFT data, shows large-scale uplift starting from 160
422 Ma to 140 Ma, a slow uplift phase from 140 Ma to 64 Ma, and then a
423 rapid uplift event. Since the temperature at 64 Ma is beyond the
424 AFT-sensitive temperature range, the thermal history model of well Z1,
425 especially for the later stages of uplift and cooling, is more reliably
426 constrained by the dual-dating sample Z1-33. The AFT simulation of
427 sample LT1-20 reveals an uplift event between 60 Ma and 55 Ma, and the
428 AHe thermal history simulation of sample ZT2-18 similarly shows an
429 uplift event from 62 Ma to 52 Ma. This indicates an early Cenozoic
430 tectonic cooling event in the region. For the T1-5 sample, located in the
431 Tianhuan syncline, uplift began at the end of the Early Cretaceous. This
432 area previously had a complete sedimentary sequence and extensive
433 sediment distribution, forming the thick Tianhuan syncline in the Ordos
434 Basin (Zhao et al., 2007a).

435 **5.2 Transformation of the Meso-Cenozoic Tectonic Regime and**



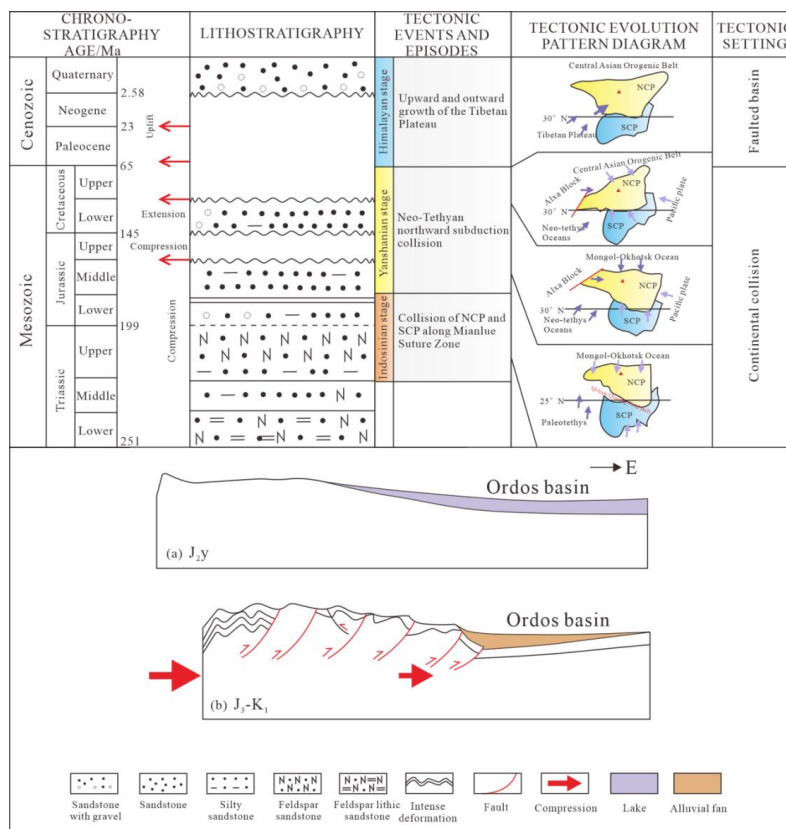
436 **Regional Dynamic Background in the North-Central Western**
437 **Margin**

438 At the end of the Paleoproterozoic, the Ordos Block formed and
439 merged with the North China Craton. Following this, under an
440 extensional tectonic environment, large-scale rifting occurred, creating
441 northeast-trending rift troughs with some structural inheritance from the
442 basement. These troughs were subsequently covered by stratigraphic
443 deposits from different periods (Bao et al., 2019; Zhao et al., 2019). In the
444 Early Paleozoic, the Ordos region transitioned into a stable cratonic basin.
445 During multiple marine transgressions and regressions, a set of
446 widespread marine carbonate sediments, interbedded with clastic rocks,
447 was deposited across the region. The large-scale Caledonian orogeny
448 caused a depositional hiatus between the Ordovician and Carboniferous
449 systems, resulting in an unconformable contact between the two. Since
450 the Late Paleozoic, the Ordos Basin has transitioned from marine to
451 terrestrial facies deposition, evolving from a coastal-continental margin to
452 shallow marine sediments, dominated by swamp, deltaic, and fluvial
453 deposits. During the Late Triassic to Early Cretaceous, the basin saw
454 intracratonic fluvial-lacustrine sedimentation. Since the Late Cretaceous,
455 the basin has experienced overall uplift and surrounding faulting. From
456 the Late Mesozoic, the Ordos Basin became an independent sedimentary
457 basin. Its sedimentary evolution has been primarily influenced by the



458 Mesozoic-Cenozoic tectonic systems, undergoing multiple sedimentary
459 cycles and uplift-related transformations (Fig. 8).

460 The Yanshanian orogeny was the primary tectonic deformation
461 period for the Ordos Basin, with the Late Jurassic tectonic movements
462 being particularly intense. These movements caused the Jurassic and
463 underlying sedimentary layers to become involved in widespread
464 deformation, resulting in a clear angular unconformity with the overlying
465 strata. This deformation was especially pronounced along the western
466 margin of the basin, where much of the surface deformation that is
467 observed today had already taken shape during this period (Darby et al.,
468 2002). In the Early Cretaceous, the deep thermal material in the basin
469 began to upwell, and the upper crust entered a tensional tectonic
470 environment. Since the Late Cretaceous, the Ordos Basin has experienced
471 significant uplift and erosion, a process that has continued to the present
472 day (Ren et al., 2007, 2008, 2014, 2017, 2020, 2022).



473

474 Fig.8 Dynamic model diagram of the northern part of the western margin of
 475 Ordos Basin.(Modified from Ma, 2019; Zhang et al., 2021; Peng et al., 2022)

476 During the Triassic period, the Indosinian Orogeny significantly
 477 impacted the region, leading to the final closure of the ancient
 478 Qinling-Qilian Ocean Basin. The continuous collision and compression
 479 of mountain ranges caused uplift and sedimentary hiatuses. As a result,
 480 the Late Triassic and Early Jurassic strata exhibit a **parallel unconformity**
 481 (Zhang et al., 2001).

482 In the Late Jurassic, the Yanshanian orogeny triggered the first major
 483 large-scale uplift in the study area. During this period, the compressional
 484 forces that were primarily north-south oriented during the earlier



485 Indosinian orogeny transitioned to an east-west orientation characteristic
486 of the Yanshanian phase (Dong et al., 2007, 2008, 2015; Zhang et al.,
487 2008). This tectonic uplift event aligns with the peak ages obtained from
488 fission tracks at 170 Ma, 161 Ma, and 153 Ma. The tectonic evolution of
489 this phase was controlled by several factors, notably the southwest Tethys
490 tectonic domain, eastward compression from the Alxa Block , and the
491 closure of the Okhotsk Ocean in the north during the Late Jurassic (Zhao
492 et al., 2023). Additionally, far-field effects from the subduction of the
493 Pacific Plate played a role (Darby et al., 2002, 2007; Faure et al., 2012;
494 Liu et al., 1998; Yang et al., 2008; Zhang et al., 2020, 2021, 2022; Zhao et
495 al., 2023). Previous paleomagnetic studies revealed that the Ordos Basin
496 was undergoing a counterclockwise rotation during this period (Ma et al.,
497 1993; Yang et al., 1999; Zhang et al., 2000). These regional tectonic
498 processes collectively shaped the large-scale uplift and deformation seen
499 during this period, marking a significant phase in the area's geological
500 history. The comprehensive analysis of stress fields in the Late Jurassic
501 indicates that multiple tectonic blocks around the Ordos Basin
502 experienced subduction, collision, compression, and even mutual rotation.
503 These interactions led to the folding and uplift of Jurassic strata,
504 accompanied by a series of imbricate thrust faults pushing from west to
505 east (Zhao et al., 1987; Ma et al., 2019; Zhang et al., 2021, 2022). In the
506 northern section, the collision with the Alxa Block initiated significant



507 uplift, while in the southern part, the overall uplift of the Qilian
508 Mountains and its thrusting into the basin resulted in strong thrusting
509 structures. This contributed to the earlier onset of uplift in areas like
510 Zhuozishan Mt. and the Majiatan-Huianbao regions. The compressional
511 deformation shows a general pattern of stronger uplift and deformation in
512 the west and at the margins, with weaker effects in the interior of the
513 basin.

514 The Early Cretaceous was a crucial period in the evolution of the
515 Ordos Basin. Northern China was under an extensional tectonic regime,
516 linked to the broader lithospheric thinning and basin development of the
517 North China Craton during the Early Cretaceous (Ren et al., 2020). In the
518 central Taole region, extensional faults from this period are observable in
519 seismic profiles (Zhao et al., 2007a). Towards the end of the Early
520 Cretaceous, the regional tectonic stress field reversed due to the multiple
521 phases of the Yanshanian orogeny (phases II, III, IV). The area was
522 simultaneously influenced by the northward collision of the Yangtze Plate
523 and the far-field effects of the Pacific Plate. The northern region was
524 affected by the closure of the Okhotsk Ocean, and the western region
525 continued to experience direct compression from the eastward movement
526 of the Alxa Block (Yang et al., 2008; Zhang et al., 2020, 2022; Zhao et al.,
527 2023). The previously deposited strata experienced intensified folding
528 and uplift under compressional stress, ~~resulting in significant structural~~



529 ~~deformation~~. This led to the formation of large-scale south-north-oriented
530 thrust faults and imbricate thrust structures. By this time, the region's
531 major tectonic framework had largely formed, and subsequent tectonic
532 movements primarily modified this existing structure.

533 During the Cenozoic, the tectonic deformation of the Ordos Basin
534 was primarily driven by the collision between the Indian and Eurasian
535 plates, with significant tectonic activity occurring during the Eocene to
536 Miocene. The continued Himalayan orogeny caused strong tectonic
537 movements in the region, leading to further uplift of the mountains, with
538 the strata predominantly displaying parallel and angular unconformities.
539 This tectonic activity has significantly shaped the present-day landscape.
540 The neighboring Alxa region, located at the northeastern edge of the
541 Tibetan Plateau, was affected by the plateau's Cenozoic uplift. Its
542 deformation is closely linked to the evolution of the Tibetan Plateau
543 (Zhang et al., 2023; Rao et al., 2016; Lei et al., 2022). Concurrently, the
544 Pacific Plate continued its northwestward subduction during this period.
545 Numerous geochronological records document the uplift and
546 northeastward expansion of the northeastern Tibetan Plateau during the
547 Cenozoic, particularly in the Eocene and Miocene (England and
548 Housemann, 1986; Tapponnier et al., 2001; Wang et al., 2008; Lease et al.,
549 2011, 2012; Craddock et al., 2011; Ding et al., 2022; Peng et al., 2019;
550 Zhao et al., 2023; Chen et al., 2024; Zhang et al., 2020). Low-temperature



551 thermochronology data, along with thermal history reconstructions
552 constrained by AHe and AFT, reveal rapid uplift during the Eocene to
553 Miocene, likely a result of the far-field effects of the Cenozoic uplift of
554 the northeastern Tibetan Plateau and the northwestward subduction of the
555 Pacific Plate.

556 Overall, the study area has undergone the Indosinian, Yanshanian,
557 and Himalayan orogenys since the Mesozoic era. The Indosinian tectonic
558 stress originated from the collision and docking of the South China Plate
559 and the North China Plate during the Triassic period, resulting in a
560 north-south stress field. The tectonic stress of the Yanshanian orogeny
561 originated from the Tethys tectonic domain, eastward compression of the
562 Alxa block, westward subduction of the Pacific plate, and closure of the
563 Okhotsk Ocean. In the northern part of the western margin of the basin,
564 the Alxa rigid block sandwiched between the South China and North
565 China plates is squeezed out in a southeast direction, directly affecting the
566 Helanshan Mountains and the northern part of the western margin of the
567 basin, causing the stress direction to shift towards a nearly east-west
568 direction. The direction of the tectonic stress field in the Himalayan
569 orogeny is influenced by the combined action of the Pacific Plate and the
570 Tethys tectonic domain, changing from a north-south direction to a
571 northeast direction. The main source of stress is the Tethys tectonic
572 domain in the southwestern part of the study area.



573 **6 Conclusion**

574 (1) This study utilizes Apatite Fission Track (AFT) and Apatite
575 (U-Th)/He (AHe) dating methods, combined with thermal history
576 modeling ~~and existing geological evidence~~, to precisely constrain the
577 uplift and cooling history of the central and northern sections of the
578 western Ordos Basin. The analysis reveals significant differences in the
579 timing and intensity of uplift across different regions: Zhuozishan part
580 experienced a large-scale uplift during the Late Jurassic (160-150 Ma),
581 followed by slow uplift between 130-30 Ma, and a more intense uplift
582 phase after 30 Ma; Taole-Hengshanbao part began uplifting around
583 155-145 Ma, followed by a period of slow uplift between 145-30 Ma, and
584 experienced another phase of rapid uplift after 30 Ma; Majiatan-Huianbao
585 part experienced a significant uplift between 158-137 Ma, with a slower
586 uplift phase from 137-110 Ma, and a period of rapid uplift again between
587 70-50 Ma. Overall, the northern and southern sections began uplifting
588 earlier, while the middle section initiated uplift slightly later. These
589 findings highlight the spatial variation in uplift timing and rates within
590 the western Ordos Basin.

591 ~~(2) This study effectively reveals the uplift movements of the~~
592 ~~northern section of the western margin during the Mesozoic and Cenozoic~~
593 ~~using low-temperature thermochronology method.~~ It suggests that the
594 Yanshanian orogeny had the most significant tectonic impact on the study



595 area. Multiple uplift events during the Mesozoic are responses to the
596 multi-phase Yanshanian orogeny in this region. Since the Cenozoic, rapid
597 uplift influenced by the Himalayan orogeny has shaped the current
598 landscape.

599 **Competing interests**

600 The contact author has declared that none of the authors has any
601 competing interests.

602 **Acknowledgements**

603 Financial support for this study were jointly provided by the Major
604 Projects of Changqing Oilfield Company (ZDZX2021). Our heartfelt
605 gratitude is given to those anonymous reviewers for their scientific and
606 linguistic revisions to the manuscript.

607 **Conferences**

- 608 [1] Bao Hongping, Shao Dongbo, Hao Songli, et al. Basement Structure and Early
609 Sedimentary Cover Evolution of the Ordos Basin[J]. Earth Science Frontiers, 2019,
610 26(1): 33-43.
- 611 [2] Barbarand J, Carter A, Wood I, et al. Compositional and structural control of
612 fission-track annealing in apatite[J]. Chemical Geology, 2003, 198(1-2): 107-137.
- 613 [3] Carlson W D, Donelick R A, Ketcham R A. Variability of apatite fission-track
614 annealing kinetics: I. Experimental results[J]. American mineralogist, 1999, 84(9):
615 1213-1223.
- 616 [4] Chen G M, Qin H T, Huang X F, et al. Cenozoic tectonic evolution of the Liupan
617 Shan area: Evidence from zircon and apatite fission tracks[J]. Chinese Journal of
618 Geophysics, 2024, 67(3): 1147-1168.
- 619 [5] Chen Gang, Wang Zhiwei, Bai Guojun, Sun Jianbo, Zhang Huiruo, Li Xiangdong.
620 Peak Age Events and Their Sedimentary-Tectonic Responses in the
621 Mesozoic-Cenozoic Ordos Basin[J]. Geology in China, 2007(03): 375-383.
- 622 [6] Chen Gang. Composition of Mesozoic Terrigenous Clastic Rocks and Their
623 Tectonic Attributes in the Ordos Basin[J]. Acta Sedimentologica Sinica, 1999(03):
624 409-413.
- 625 [7] Craddock W, Kirby E, Zhang H P. 2011. Late Miocene-Pliocenerange growth in



- 626 the interior of the northeastern Tibetan Plateau, *Lithosphere*, 3(6):420-438.
- 627 [8] Darby B J, Ritts B D. Mesozoic contractional deformation in the middle of the
628 Asian tectonic collage: the intraplate Western Ordos fold-thrust belt, China[J]. *Earth
629 and Planetary Science Letters*, 2002, 205(1-2): 13-24.
- 630 [9] Darby B J, Ritts B D. Mesozoic structural architecture of the Lang Shan,
631 North-Central China: Intraplate contraction, extension, and synorogenic
632 sedimentation[J]. *Journal of Structural Geology*, 2007, 29(12): 2006-2016.
- 633 [10] Ding L, Kapp P, Cai F, et al. Timing and mechanisms of Tibetan Plateau uplift[J].
634 *Nature Reviews Earth & Environment*, 2022, 3(10): 652-667.
- 635 [11] Dong Shuwen, Zhang Yueqiao, Chen Xuanhua, et al. Formation and
636 Deformation Characteristics of the Late Jurassic Multidirectional Convergent Tectonic
637 System in East Asia[J]. *Acta Geoscientia Sinica*, 2008, 29(3): 306-317.
- 638 [12] Dong Shuwen, Zhang Yueqiao, Li Hailong, et al. The "Yanshan Movement" and
639 the Late Mesozoic Multiplate Convergence Tectonics in East Asia: Commemorating
640 the 90th Anniversary of the "Yanshan Movement"[J]. *Science in China: Earth
641 Sciences*, 2019, 49(6): 913-938.
- 642 [13] Dong Shuwen, Zhang Yueqiao, Long Changxing, et al. New Interpretations of
643 the Jurassic Tectonic Transformations and the Yanshan Movement in China[J]. *Acta
644 Geologica Sinica*, 2007, 81(11): 1449-1461.
- 645 [14] Dong Yunpeng, Li Wei, Zhang Feifei, et al. Formation and Evolution of the
646 Helan Mountain in the Northern Section of the North-South Tectonic Belt[J]. *Journal
647 of Northwest University (Natural Science Edition)*, 2021, 51(6): 951-968
- 648 [15] England P, Houseman G, 1986. Finite strain calculations of
649 continental deformation: 2. Comparison with the India-Asia Collision Zone. *Journal of
650 Geophysical Research: Solid Earth*, 91(B3):3664-3676.
- 651 [16] Farley K A, Wolf R A, Silver L T. The effects of long alpha-stopping distances
652 on (U-Th)/He ages[J]. *Geochimica et cosmochimica acta*, 1996, 60(21): 4223-4229.
- 653 [17] Faure M, Lin W, Chen Y. Is the Jurassic (Yanshanian) intraplate tectonics of
654 North China due to westward indentation of the North China block?[J]. *Terra Nova*,
655 2012, 24(6): 456-466.
- 656 [18] Flowers R M, Farley K A, Ketchum R A. A reporting protocol for
657 thermochronologic modeling illustrated with data from the Grand Canyon[J]. *Earth
658 and Planetary Science Letters*, 2015, 432: 425-435.
- 659 [19] Gallagher K. Transdimensional inverse thermal history modeling for quantitative
660 thermochronology[J]. *Journal of Geophysical Research: Solid Earth*, 2012, 117(B2).
- 661 [20] Gan Kewen. On the Genesis Mechanism of Thrust Belts and Hydrocarbon
662 Prospects of the Western Margin of the Ordos Basin[J]. In: Yang Junjie. *Thrust
663 Tectonics and Hydrocarbon in the Western Ordos Basin*. Lanzhou: Gansu Science and
664 Technology Press, 1990, 31239.
- 665 [21] Gao Feng, Wang Yuejun, Liu Shunsheng, Hu Baoqing. Study on the Thermal
666 History of the Western Margin of the Ordos Basin Using Apatite Fission Track
667 Analysis[J]. *Geotectonica et Metallogenia*, 2000(01): 87-91.
- 668 [22] Gao Shaohua. Mesozoic-Cenozoic Evolutionary Modification of the Lateral
669 Structural Belt in the Central Western Ordos Basin and Its Significance for Oil and



- 670 Gas[D]. Xi'an: Northwest University, 2014.
- 671 [23] Gleadow A J W, Seiler C, Rink W J, et al. Fission track dating and
672 thermochronology[J]. Encyclopedia of scientific dating Methods, 2015: 285-296.
- 673 [24] Hasebe N, Barbarand J, Jarvis K, et al. Apatite fission-track chronometry using
674 laser ablation ICP-MS[J]. Chemical Geology, 2004, 207(3-4): 135-145.
- 675 [25] He Dengfa, Sun Fangyuan, Zhai Yonghe, et al. Formation Evolution of the
676 Shigouyi Anticline in the Western Ordos Basin and Its Tight Sandstone Gas
677 Accumulation Model[J]. Oil & Gas Geology, 2021, 42(2): 370-390.
- 678 [26] Jiang Suyang, Huang Wenhui, Zhang Yongsheng, et al. Tectonic Setting and
679 Provenance Analysis of the Sandstones from the Sandaokan Formation in the
680 Northern Segment of the Western Ordos Basin[J]. Journal of Northeast Petroleum
681 University, 2019, 43(4): 17-28.
- 682 [27] Ketcham R A, Carter A, Donelick R A, et al. Improved modeling of fission-track
683 annealing in apatite[J]. American Mineralogist, 2007, 92(5-6): 799-810.
- 684 [28] Ketcham R A. Forward and inverse modeling of low-temperature
685 thermochronometry data[J]. Reviews in mineralogy and geochemistry, 2005, 58(1):
686 275-314.
- 687 [29] Lease R O, Burbank D W, Hough B, et al. 2012. Pulsed Miocene growth in
688 northeastern Tibet: insights from Xunhua Basin magnetostratigraphy and provenance.
689 GSA Bull., 124(5-6):657-677.
- 690 [30] Lease R.O., Burbank D W, Clark M K, et al. 2011. Middle
691 Miocene reorganization of deformation along the northeastern Tibetan Plateau,
692 Geology, 39(4):359-362.
- 693 [31] Lei Q, Yu J, Zhang P, et al. Tectonic geomorphology and prehistoric earthquakes
694 of the West Helanshan fault, West Ordos, and its implications for regional tectonics
695 and seismic hazard[J]. Tectonophysics, 2022, 833: 229375.
- 696 [32] Li Bin. Study on the Thrust Belt Structure and Hydrocarbon Controlling Factors
697 in the Western Ordos Basin[D]. Northwest University, 2019.
- 698 [33] Li Bin. Tectonic Characteristics and Hydrocarbon Accumulation Studies of the
699 Foreland Basin in the Western Ordos Basin[D]. Graduate School of the Chinese
700 Academy of Sciences (Guangzhou Institute of Geochemistry), 2006.
- 701 [34] Li Tianbin. Characteristics and Evolution of Thrust Structures in the Western
702 Ordos Basin[D]. China University of Geosciences (Beijing), 2006.
- 703 [35] Liu Chiyang, Zhao Hongge, Wang Feng, et al. Mesozoic Tectonic
704 Characteristics of the Western Margin of the Ordos Basin[J]. Acta Geologica Sinica,
705 2005, 79(6): 737-747.
- 706 [36] Liu Hefu. Types of Foreland Basins and Styles of Fold-Thrust Structures[J].
707 Earth Science Frontiers, 1995, 2(3): 59-68.
- 708 [37] Liu Jianhui. Cenozoic Extensional Uplift of the Helan Mountains and Qinling
709 Mountains and Analysis of Fault Frictional Heating Using Apatite Fission Track
710 Method[J]. International Seismological Dynamics, 2010, 31(3): 31-33.
- 711 [38] Liu S F, The coupling mechanism of basin and orogen in the western ordos
712 Basin and adjacent regions of China[J]. Journal of Asian Earth
713 Science, 1998, 16(4):369-383.



- 714 [39] Liu Shaofeng, Yang Shigong. North-South Differences and Their Formation
715 Mechanism on the Western Margin of the Ordos Basin[J]. Geological Science, 1997,
716 32(3): 397-408.
- 717 [40] Ma Jinghui, He Dengfa. Mesozoic-Cenozoic Tectonic Events in the Helan
718 Mountain Tectonic Belt and Adjacent Areas: Constraints from Unconformities and
719 Fission Track Analysis[J]. Acta Petrologica Sinica, 2019, 35(4): 1121-1142.
- 720 [41] Ma X.H., Xing L.S., Yang Z.Y., et al. Paleomagnetic Study of the Ordos Basin
721 since the Late Paleozoic [J]. Chinese Journal of Geophysics, 1993, (01): 68-79.
- 722 [42] Ouyang Zhengjian, Chen Hongde, Feng Juanping. Tectonic Characteristics and
723 Evolution of the Central and Southern Segments of the Western Margin of the Ordos
724 Basin[J]. Modern Geology, 2012, 26(04): 691-695.
- 725 [43] Peng H , Wang J , Liu C ,et al. Thermochronological constraints on the
726 Meso-Cenozoic tectonic evolution of the Haiyuan-Liupanshan region, northeastern
727 Tibetan Plateau[J]. Journal of Asian earth sciences, 2019,
728 183(Oct.1):103966.1-103966.13.
- 729 [44] Peng H, Wang J, Liu C, et al. Mesozoic exhumation and ca. 10 Ma reactivation
730 of the southern Yin Shan, North China, revealed by low-temperature
731 thermochronology[J]. Tectonophysics, 2022, 823: 229189.
- 732 [45] Peng Heng. Fission Track Thermochronology Analysis and Its Geological
733 Significance in the Southwestern Adjacent Area of the Ordos Block[D]. Northwest
734 University, 2020.
- 735 [46] Rao G, Chen P, Hu J, et al. Timing of Holocene paleo-earthquakes along the
736 Langshan Piedmont Fault in the western Hetao Graben, North China: Implications for
737 seismic risk[J]. Tectonophysics, 2016, 677: 115-124.
- 738 [47] Ren Zhanli, Cui Junping, Qi Kai. New Advances in the Theoretical Research and
739 Methods for Restoring the Thermal Evolution History of Deep and Ultra-deep Layers
740 in Overlapping Basins[J]. Journal of Northwest University (Natural Science Edition),
741 2022, 52(6): 910-929.
- 742 [48] Ren Zhanli, Liu Li, Cui Junping, et al. Application of Tectonic Thermal
743 Evolution History in the Study of Hydrocarbon Accumulation Phases[J]. Oil & Gas
744 Geology, 2008, 29(4): 502-506.
- 745 [49] Ren Zhanli, Qi Kai, Liu Runchuan, et al. The Dynamical Background of Early
746 Cretaceous Tectonic Thermal Events in the Ordos Basin and Their Control on the
747 Accumulation Periods of Various Minerals, Including Oil and Gas[J]. Acta
748 Petrologica Sinica, 2020, 36(4): 1213-1234.
- 749 [50] Ren Zhanli, Tian Tao, Li Jinbu, et al. Research Methods for Thermal Evolution
750 History of Sedimentary Basins and Progress in Reconstructing Thermal Evolution
751 History of Overlapping Basins[J]. Journal of Earth Sciences and Environment, 2014,
752 36(3): 1-20.
- 753 [51] Ren Zhanli, Yu Qiang, Cui Junping, Qi Kai, Chen Zhanjun, Cao Zhanpeng, Yang
754 Peng. Thermal Evolution History of the Ordos Basin and Its Control on
755 Hydrocarbons[J]. Earth Science Frontiers, 2017, 24(03): 137-148.
- 756 [52] Ren Zhanli, Zhang Sheng, Gao Shengli, Cui Junping, Xiao Yuanyuan, Xiao Hui.
757 Tectonic Thermal Evolution History of the Ordos Basin and Its Significance for



- 758 Accumulation and Mineralization[J]. *Science in China: Series D, Earth Sciences*,
759 2007(S1): 23-32.
- 760 [53] Ren Zhanli. Study on the Geothermal History of the Ordos Basin Using the
761 Apatite Fission Track Method[J]. *Chinese Journal of Geophysics*, 1995, 38(03):
762 339-349..
- 763 [54] Tang Xiyuan, Guo Zhongming, Wang Dingyi. Characteristics, Evolution, and
764 Hydrocarbon Exploration of the Thrust Nappe Structure Belt in the Western Ordos
765 Basin[J]. *Oil & Gas Geology*, 1988, 9(1): 1-10.
- 766 [55] Tang Xiyuan. Thrust Nappe Structures and Hydrocarbon Exploration on the
767 Western Margin of the Shaanxi-Gansu-Ningxia Basin[M]. Xi'an: Northwest
768 University Press, 1992.
- 769 [56] Tapponnier P, XuZ Q, Roger F, et al. 2001. Oblique stepwise rise and growth of
770 the Tibet Plateau. *Science*, 294(5547):1671-1677.
- 771 [57] Tian Chaoyang, Chen Hong, Liu Xinshe, et al. Fission Track Ages and Mesozoic
772 Tectonic Uplift in the Niushou Mountain—Luoshan Area of the Western Ordos[J].
773 *Journal of Geological Mechanics*, 2023, 29(05): 599-617.
- 774 [58] Vermeesch P. RadialPlotter: A Java application for fission track, luminescence
775 and other radial plots[J]. *Radiation Measurements*, 2009, 44(4): 409-410.
- 776 [59] Wang CS, Zhao XX, Liu ZF, et al. 2008. Constraints on the early uplift history of
777 the Tibetan Plateau, *Proc, Natl. Acad. Sci. USA*, 105(13):4987-4992
- 778 [60] Yang Hua, Fu Jinhua, Ouyang Zhengjian, Sun Liuyi. Analysis of
779 Tectonic-Sedimentary Environments during the Late Triassic in the Western Margin
780 of the Ordos Basin[J]. *Acta Sedimentologica Sinica*, 2011, 29(03): 427-439.
- 781 [61] Yang J.J., Zhang B.R. Basic Characteristics of the Overthrust Belt on the
782 Western Margin of the Ordos Basin[A]. In: Yang J.J., Zhao Z.Y., Liu H.F., et al.
783 Structure and Oil and Gas of the Overthrust Belt on the Western Margin of the Ordos
784 Basin[C]. Lanzhou: Gansu Science and Technology Press, 1990. 91-105.
- 785 [62] Yang Junjie, Zhang Borong. Strike-Slip Rift and Associated Thrust Belt: A Case
786 Study of the Yinchuan Graben and Hengshanpu Thrust Belt[J]. *Petroleum Exploration
787 and Development*, 1986(02): 1-8.
- 788 [63] Yang S.B., Geng X.X., Guo Q.Y., et al. Mesozoic Tectonic Evolution in the
789 Northern Section of the Western Margin of the Ordos Basin[J]. *Geological Review*,
790 2008, 54(3): 307-315.
- 791 [64] Yang Shengbin, Geng Xinxia, Guo Qingyin, et al. Mesozoic Tectonic Evolution
792 of the Northern Segment of the Western Ordos Basin[J]. *Geological Review*, 2008,
793 54(3): 307-315.
- 794 [65] Yang Shengbin, Guo Qingyin, Hou Guiting, et al. Subsidence History and
795 Sedimentary Response in the Northern Segment of the Western Ordos Basin[J].
796 *Journal of Peking University: Natural Science Edition*, 2006, 42(2): 192-198.
- 797 [66] Zhai Mingguo. The Formation, Evolution, and Metallogenesis of the North
798 China Craton[J]. *Mineral Deposits*, 2010 (1): 24-36.
- 799 [67] Zhai Mingguo. The Ordos Block: The Key to Unraveling the Mysteries of Early
800 Continental Formation, Evolution, and Tectonic Regime of the North China Craton[J].
801 *Chinese Science Bulletin*, 2021, 66(26): 3441-3461.



- 802 [68] Zhang Chengli, Gou Longlong, Liu Xinyu, et al. Precambrian Geological Events,
803 Nature, and Geological Significance of the Basement in the Western North China
804 Craton[J]. *Acta Petrologica Sinica*, 2018, 34(4): 981-998.
- 805 [69] Zhang Guowei, Dong Yunpeng, Yao Anping. A New Starting Point for the Study
806 of Orogenic Belts and Orogenesis[J]. *Northwest Geology*, 2001, 34(1): 1-9.
- 807 [70] Zhang J, Cunningham D, Qu J, et al. Poly-phase structural evolution of the
808 northeastern Alxa Block, China: Constraining the Paleozoic-Recent history of the
809 southern central Asian Orogenic belt[J]. *Gondwana Research*, 2022, 105: 25-50.
- 810 [71] Zhang J, Wang Y, Qu J, et al. Mesozoic intracontinental deformation of the Alxa
811 Block in the middle part of Central Asian Orogenic Belt: A review[J]. *International
812 Geology Review*, 2021, 63(12): 1490-1520.
- 813 [72] Zhang J, Yun L, Zhang B, et al. Deformation at the easternmost Altyn Tagh Fault:
814 Constraints on the growth of the northern Qinghai–Tibetan plateau[J]. *Acta Geologica
815 Sinica-English Edition*, 2020, 94(4): 988-1006.
- 816 [73] Zhang J., Ma Z.J., Ren W.J. Mechanism of North-South Differences in the
817 Overthrust Belt on the Western Margin of the Ordos Basin[J]. *Geotectonica et
818 Metallogenia*, 2000(02): 124-133.
- 819 [74] Zhang Jiasheng, He Zixin, Fei Anqi, et al. Large Margin Thrust Nappe System in
820 the Northern Segment of the Western Ordos Basin[J]. *Geological Science*, 2008, 43(2):
821 251-281.
- 822 [75] Zhang Jin, Zhang Beihang, Zhao Heng, et al. Characteristics and Mechanisms of
823 Late Cenozoic Deformation in the Beishan-Alashan Region[J]. *Earth Science
824 Frontiers*, 2023, 30(5): 334.
- 825 [76] Zhao Chongyuan, Liu Chiyang, Ren Zhanli. Geology of Oil and Gas Basins and
826 System Engineering in Their Research[J]. *Oil & Gas Geology*, 1990, 11(1): 108-113.
- 827 [77] Zhao D., Chen P., Li R.X., et al. Basin Records of Multistage Tectonic Uplift in
828 the Longshou Mountain of the Northeastern Tibetan Plateau during the Late Cenozoic
829 [J]. *Acta Petrologica Sinica*, 2023, 39(12): 3759-3774.
- 830 [78] Zhao Hongge, Liu Chiyang, Wang Feng, et al. Tectonic Partitioning and
831 Characteristics of the Western Margin of the Ordos Basin[J]. *Oil & Gas Geology*,
832 2006, 27(2): 173-179.
- 833 [79] Zhao Hongge, Liu Chiyang, Wang Feng, et al. Uplift Timing and Evolution of
834 the Helan Mountains[J]. *Science in China: Series D*, 2007, 37(A01): 185-192.
- 835 [80] Zhao Hongge, Liu Chiyang, Wang Jianqiang, et al. Exploration of Tectonic
836 Attributes during the Late Triassic in the Western Ordos Basin[J]. *Geological Journal
837 of China*, 2007, 34(3): 384-391.
- 838 [81] Zhao Hongge, Liu Chiyang, Yao Yaming, Wang Feng, Yin Yan. Fission Track
839 Evidence of Differential Uplift in the Western Ordos Basin[J]. *Journal of Northwest
840 University (Natural Science Edition)*, 2007, (03): 470-474.
- 841 [82] Zhao Hongge. Tectonic Characteristics and Evolution of the Western Ordos
842 Basin[D]. Northwest University, 2003.
- 843 [83] Zhao Pan, Xu Bei, Chen Yan. Mongolian–Okhotsk Ocean: Evolutionary Process
844 and Final Closure[J]. *Science in China: Earth Sciences*, 2023, 53(11): 2541-2559.
- 845 [84] Zhao X, Coe R S. 1987.Palaeomagnetic constraints on the collision and rotation



846 of North and South China. *Nature*, 327:41-144.
847 [85] Zhao Xiaochen. *Mesozoic Tectonic Evolution and Later Modification of the*
848 *Northern Section of the North-South Tectonic Belt in China*[D]. Xi'an: Northwest
849 University, 2017.
850 [86] Zhao Y, Liu X, Hu J, et al. Metamorphism of diverse basement gneisses of the
851 Ordos Basin: Record of multistage Paleoproterozoic orogenesis and constraints on the
852 evolution of the western North China Craton[J]. *Precambrian Research*, 2019, 328:
853 48-63.
854 [87] Zhuo Yuzhou. *Determination of Mesozoic-Cenozoic Uplift Events in the*
855 *Zhuozishan Area of the Northwestern Ordos Basin and Their Tectonic*
856 *Significance*[D]. Northwest University, 2015.
857